Structural analyses of von Willebrand factor C domains of collagen 2A and CCN3 reveal an alternative mode of binding to bone morphogenetic protein-2*

Emma-Ruoqi Xu[1,2], Emily E. Blythe[1,3], Gerhard Fischer and Marko Hyvönen[4]

Department of Biochemistry, University of Cambridge, 80 Tennis Court Road,
Cambridge CB2 1GA, United Kingdom

*Running title: BMP-2 binding of vWC domains of Collagen IIA and CCN3

[1] These authors contributed equally
[2] Current address: EMBL c/o DESY, Notkestraße 85, Hamburg 22607, Germany
[3] Current address: California Institute of Technology, 1200 E. California Blvd, MC 114-96, Pasadena, CA, 91125, USA
[4] To whom correspondence should be addressed: Marko Hyvönen, email: mh256@cam.ac.uk

ABSTRACT

Bone morphogenetic proteins (BMPs) are secreted growth factors that promote differentiation processes in embryogenesis and tissue development. Regulation of BMP signalling involves binding to a variety of extracellular proteins, among which are many von Willebrand factor C (vWC) domain-containing proteins. While the crystal structure of the complex of crossveinless-2 (CV-2) vWC1 and BMP-2 previously revealed one mode of the vWC:BMP binding mechanism, other vWC domains may bind to BMP differently. Here, using X-ray crystallography, we present for the first time structures of the vWC domains of two proteins thought to interact with BMP-2— collagen IIA and matricellular protein CCN3. We found that these two vWC domains share a similar N-terminal fold that differs greatly from that in CV-2 vWC, which comprises its BMP-2-binding site. We analysed the ability of these vWC domains to directly bind to BMP-2 and detected an interaction only between the collagen IIa vWC and BMP-2. Guided by the collagen IIa vWC domain crystal structure and conservation of surface residues among orthologous domains, we mapped the BMP-binding epitope on the subdomain 1 of the vWC domain. This binding site is different from that previously observed in the complex between CV-2 vWC and BMP-2, revealing an alternative mode of interaction between vWC domains and BMPs.

Bone morphogenetic proteins (BMPs) are members of the TGF-β superfamily, a group of extracellular growth factors that play important roles in embryonic patterning, differentiation, and homeostasis of various tissue types (1). Many biological processes rely on the normal functioning of BMPs, including the development and maintenance of cartilage and bones, wound repair, and tissue homeostasis, whereas perturbations of BMP signalling are implicated in diseased states such as fibrosis, vascular diseases, and cancer progression (2–8). Secreted dimeric BMPs signal these processes through binding of two type I and two type II serine/threonine kinase receptors, which in turn phosphorylate Smad 1/5/8 proteins and MAP kinases to ultimately regulate gene expression (9). Furthermore, the regulation of BMP signalling involves direct binding by a range of extracellular proteins, including Follistatin, Gremlins, and Noggin, that inhibit the receptor-mediated activity of BMPs (10–15).

Many regulatory proteins, such as the Chordin family members Crossveinless-2 (CV-2), Chordin, and Chordin-like 2 (CHL2), bind BMPs through von Willebrand factor C (vWC) domains. The vWC domain, originally identified in the von Willebrand factor (16), typically contains 75-100 residues, with ten conserved cysteines. Two cysteine-containing

motifs, C*XX*C*X*C and CC*XX*C, lie toward the middle and the C-terminal parts of the domain, respectively (17). X-ray crystallographic and NMR structures have revealed that vWC domains comprise an N-terminal region, and two subdomains of SD1 and SD2 linked together by a disulfide bond (17, 18). CV-2, Chordin, and CHL2 each contain multiple vWC domains that interact with BMPs with variable affinities (18–22). Moreover, the various vWC domains have been shown to interact with either or both of the types I and II receptor binding sites on BMP-2, thereby resulting in different mechanisms of inhibition of BMP signalling (18, 21, 22).

The crystal structure of the first vWC domain of CV-2 (CV-2 vWC1) in complex with BMP-2 revealed one modality of the vWC:BMP-2 interaction (18). The CV-2 vWC1 binds to BMP-2 through two separate sites of interactions. Firstly, there is high-affinity binding between its N-terminal clip and the type I receptor binding site on BMP-2 *via* hydrogen bonds, at a nanomolar affinity compatible with the type I receptor:BMP-2 interaction. As shown by its NMR structure in solution at unbound state, this BMP-2 compatible conformation of the N-terminal clip is pre-formed in the CV-2 vWC domain instead of being induced by complexation (23), suggesting that the N-terminal structure of a vWC domain could be indicative of its binding mechanism with BMPs. Secondly, there are hydrophobic interactions between its SD1 and the type II receptor binding site on BMP-2 at a similarly low affinity. The SD2 of CV-2 vWC1 was shown to make no contact with BMP-2 (18). For other BMP-binding vWC domains in Chordin and CHL2, the BMP2-binding epitopes have also been pinned down in the SD1, although structural information of their N-termini have hitherto been unavailable to compare their binding modes with that of CV-2 (22).

Two other known BMP-2-binding proteins – Collagen IIA (Col2a) and CCN3 – contain largely uncharacterised vWC domains (24–26). Col2a is an alternatively spliced form of procollagen II, expressed in mesenchymal and epithelial cells prior to differentiation (26, 27). The alternatively spliced exon encodes for a vWC domain, inserted in its non-helical N-terminal propeptide (28). This vWC domain is known to bind BMP-2 and confers anti-BMP-2 activity to Col2a in bioassays (19, 24). The solution NMR structure of Col2a vWC has shown similarities to the fibronectin type 1 domain and CV-2 vWC1 (17, 18, 29). The N-terminal part of Col2a vWC is clearly different from corresponding part of the CV-2 vWC1, suggesting that Col2a vWC binds BMP-2 through an alternative, as yet uncharacterised mechanism (18).

CCN3 (also known as Nephroblastoma overexpressed, Nov), is a member of the CCN family of matricellular proteins (30). CCN3 has been recognised as a pro-angiogenic factor, a proliferation antagonist, an inhibitor of the bone and cartilage development, a negative regulator in fibrosis, as well as being involved in various types of cancer (31–40). CCN proteins are characterised by their conserved primary structure, comprised of four clearly distinguishable disulfide-rich domains (41). The vWC domain is the second domain in the N-terminal half for CCN proteins, following the insulin-like growth factor binding (IB) domain. These two domains are separated by a hinge region from the C-terminal half that contains thrombospondin module 1 (TSP-1) and C-terminal cysteine-knot (CTCK) domains (41). While it has been demonstrated that CCN3 binds to BMP-2 (25), and that it promotes the MAP kinase signalling, possibly through BMP (42), the exact site of interaction in CCN3 is yet to be identified.

In order to understand the molecular mechanism of BMP-2 binding by Col2a and CCN3, we have determined crystal structures of vWC domains from both of these proteins and analysed their interactions with BMP-2. We observe both common and unique features in the crystal structures of these two vWC domains when compared with the existing structure of CV-2 vWC1. Our biochemical analyses demonstrate that Col2a weakly binds to BMP-2 through a novel hydrophobic interaction on the opposite side of its SD1 as compared with CV-2 vWC1. However, despite its overall structural similarities to Col2a vWC, CCN3 vWC does not bind BMP-2.

RESULTS

Crystal structures of Col2a vWC and CCN3 vWC–In order to begin to make comparisons among vWC domains, we determined the structures of the vWC domains from both Col2a and CCN3 by X-ray crystallography.

The crystal structure of Col2a vWC was determined through sulphur SAD phasing at a resolution of 1.74 Å (Table 1). Like with other

vWC domains, the domain has an elongated shape with N- and C-termini at the opposite ends. As expected, the conserved cysteines are all involved in intramolecular disulfide bonds, with the same connectivity as seen before: C_1-C_4, C_2-C_8, C_3-C_5, C_6-C_9, C_7-C_{10} (subscripted numbers refer to the sequential position of the cysteines in the vWC sequence, Fig. 1). The structure can be subdivided into three parts: an N-terminal β-hairpin region, a subdomain 1 (SD1), and a subdomain 2 (SD2; Fig. 1*A*). The N-terminal region comprises a two-stranded antiparallel β-sheet that resembles the fold of a β-hairpin, while SD1 consists of a three-stranded antiparallel β-sheet with a disulfide (C_3-C_5) between the last two strands. The angle between the N-terminal β-hairpin and SD1 is stabilised by a π-stacking interaction formed by two aromatic residues, Y41 and W47, as well as a disulfide bond (C_1-C_4) between the first strand of the β-hairpin and the second strand of SD1. SD2 is devoid of regular secondary structure, though it is tethered by one disulfide bond within itself (C_7-C_{10}) and by two disulfides to SD1 (C_2-C_8 and C_6-C_9). The two molecules in the asymmetric unit align well for most of the structure, with an overall RMSD of 0.464 Å for 49 out of 67 residues; the main differences are found in the first part of SD2 (aa. 71-77, RMSD of 1.05 Å) and in the flexible loop at the C-termini (aa. 89-96, RMSD of 2.49 Å) (Fig. S1*A*).

The structure of the Col2a vWC domain has previously been solved by NMR (17), and an alignment, using only the β-hairpin and SD1, of our crystal structure to the NMR ensemble is shown in Figure 1*B*. The β-hairpin and SD1 agree very well between the different NMR models and the crystal structure, with RMSD of 0.9-1.3 Å. However, we see much poorer overall alignment (RMSD ~3.5 Å) when comparing the entire structures or SD2 (Fig. S2). The disorder in SD2 observed in the NMR ensemble—particularly in the C-terminal tail after the last cysteine—suggests that our crystal structure captured one of many conformations possible for SD2 and that there is flexibility in both SD2 and in its relative orientation to SD1. Additionally, we observe a more extended third β-strand in SD1, a consequence of an extendedβ-sheet that is formed between the two molecules in the asymmetric unit of the crystal (Fig. S1*B*).

Meanwhile, the structure of CCN3 vWC was solved using selenomethionine labelled vWC, with mutations V105M/R128M to introduce methionines that are otherwise lacking in the domain. This experimentally derived mutant structure was then used to solve the structure of the wild type vWC domain and that was refined to 2.1 Å resolution (Table 1). Similar to Col2a vWC, the CCN3 vWC comprises an N-terminal β-hairpin, an SD1 of three β-strands, and an SD2 of three β-strands (Fig. 1*C*), stabilised by five conserved disulfide bonds with the same connectivity. The angle between the β-hairpin and SD1 is also stabilised by a π-π interaction between two aromatic side chains, Y111 and F117, and a disulfide bond (C_1-C_4). While SD2 of Col2a vWC is devoid of regular secondary structure, SD2 of CCN3 vWC consists of a three-stranded antiparallel β-sheet. All four molecules in the asymmetric unit for CCN3 vWC are nearly identical, with RMSD of 0.121-0.338 Å (Fig. S3*A*). The structure of the V105M/R128M mutant domain aligns well with the wild type vWC domain, while its packing in the crystal is very different, suggesting that the orientation between the SD1/SD2 subdomains in CCN3 is relatively stable (data not shown).

Conservation analysis of Col2a vWC and CCN3 vWC–As evolutionary conservation can reflect structural and/or functional importance of individual residues in a protein, we performed such analysis for the newly determined Col2a vWC and CCN3 vWC structures. Given the generally low conservation between different vWC domains, and possibly different molecular functions this domain has in different proteins, analysis of sequences from a single species was not deemed to be fruitful. Instead, we used a large number of orthologue sequences across different species to make sure we analyse conservation between functionally identical domains. We extracted the sequences from the Ensembl genome browser to ensure widest possible coverage of eukaryotes and removed only the sequences with significant stretches of poorly defined segments.

As expected, all ten cysteines are fully conserved across species in Col2a vWC. The two aromatic residues forming a π-π interaction in SD1, Y41 and W47 in human Col2a vWC, are also conserved for apparent structural importance. The tryptophan residue exists in all species, while the phenylalanine residue is found in all but one species (replaced by a histidine in tetraodon collagen) (Fig. S7). Besides this structural conservation at the core of the

structure, clusters of functional conservation were also observed in various surface positions. These include a hydrophobic patch in the SD1, with two valine residues (V46 and V56 in human Col2a) and a leucine residue (L63), and an isoleucine residue (I54), with three substitutions to valines. In SD2, there is another moderately conserved hydrophobic surface consisting of an isoleucine (I80), a phenylalanine (F82), and another isoleucine/valine residue (I88; Fig. 5*A* and S7).

For CCN3 vWC, the cysteines are also highly conserved across species, with only one exception. In the hedgehog CCN3, three cysteines (C_1, C_3, and C_6) out of ten appear to have mutated. This would have significant consequences for the stability of the domain as these changes break three of the five disulfides in the domain, and would disrupt the structure completely. Like in Col2a, both aromatic residues involved in the stabilisation of the N-terminal β-hairpin and SD1 are highly conserved in CCN3 vWC. The tyrosine is invariable in all but 5 out of 69 sequences, whereas the phenylalanine is even more conserved with substitutions to tyrosine found in just two species. However, unlike Col2a vWC, conservation of solvent exposed residues on the CCN3 vWC domain is less evident. The only cluster with relatively conserved residues is in the SD2. This site is comprised of P145, K153, and W165 in CCN3 vWC (Fig. S8), but in the absence of detectable binding to BMP-2 we have not studied the possible functional role of these residues.

Structural comparisons among Col2a vWC, CCN3 vWC, and CV-2 vWC1–Besides our new structures and the Col2a NMR structure, the only other vWC structure available is that of CV-2 vWC1 bound to BMP-2 (16). Figure 2*A-C* show pair-wise comparisons of these three structures (*A*, Col2a/CCN3; *B*, Col2a/CV-2; *C*, CCN3/CV-2). Generally, these three structures share common subdomain architectures and disulfide bond connections. Disulfide C_1-C_4 is between the N-terminal clip (CV-2) or the first strand of N-terminal β-hairpin (Col2a and CCN3), and the second strand of SD1. C_3-C_5 connects the second and third strand in SD1. The disulfide bond of C_2-C_8 links SD1 with SD2, while C_6-C_9 and C_7-C_{10} form inter-strand disulfide bonds at the top and bottom of the SD2, respectively. While the connectivities of the five disulfide bonds are identical in all three vWC structures, detailed comparisons reveal subtle differences in their

positions. In CCN3 vWC, only the C_1-C_4 and C_3-C_5 in the N-terminal half are in the same positions as in Col2a and CV-2 vWCs. The lack of a proline residue before the *C2* in CCN3 (P51 in Col2a and P28 in CV-2) has caused the C_2-C_8, and subsequently C_9-C_6, to shift their positions by one residue (Fig. 2*D* and S4). This proline residue is only conserved in about a quarter of all human vWC domains, suggesting these proteins will have similar spatial organisation of disulfide bonds in CCN3 vWC (Fig. S5).

While the subdomain boundaries and disulfide connectivities are conserved among the three currently available vWC structures, they display significant differences as well. The angles formed between SD1 and SD2 display great variability among the three structures, varying by up to 50°. This is not particularly surprising, as the NMR ensemble of the structures of Col2a vWC and CV-2 vWC1 domains in solution suggests significant flexibility in the linker between the subdomains. Additionally, the structural changes caused by the proline before the second cysteine (C_2) and the shift of the two disulfide positions in Col2a and CV-2 vWCs are likely to play a role in the relative orientation between SD1 and SD2. Previous investigations of CV-2 and CHL2 vWC domains have demonstrated that SD1 subdomains are responsible for BMP-2 binding, and SD2 subdomains appear to play no direct role in this (18, 22).

Superimposition of the structures shows that the N-terminal halves of Col2a vWC and CCN3 vWC domains are more similar to each other than they are to the corresponding part of CV-2 vWC1. Two major structural differences suggest that the Col2a and CCN3 vWC domains cannot bind BMP-2 in the same manner as CV-2 vWC1. Firstly, the N-terminal regions of Col2a and CCN3 vWCs have more regular secondary structures compared with that in CV-2 vWC1 (Fig. 2*A-C*). The double-stranded antiparallel β-sheet found in both Col2a vWC and in CCN3 vWC resembles a hairpin, instead of the clip-like fold in CV-2 vWC1. The angle between the N-terminal β-hairpin and SD1 is stabilised *via* a disulfide bond C_1-C_4, as well as the aromatic interaction between Y41 and W47 in Col2a, and Y111 and F117 in CCN3. While the equivalent disulfide bond is also observed in CV-2 vWC1, the aromatic residues are absent and the N-terminal part of the domain forms a more loosely

4

packed structure. As shown by Zhang *et al.* (18) the N-terminal clip of CV-2 vWC1 is very important for the high affinity binding to BMP-2 on the type I receptor binding site *via* hydrogen bonds. Even though the hydrogen bond formation is through the main chain atoms in CV-2 vWC1 and thus does not require sequence conservation, the folded β-hairpin structure in Col2a and CCN3 vWC domains would not allow their N-terminal regions to bind BMP-2 in the same manner as CV-2 vWC1. Secondly, the first of the three antiparallel strands in SD1 is part of a regular β-sheet in Col2a vWC and CCV3 vWC, whereas in CV-2 vWC1 it forms an extended loop structure that is the other major element of the interface with the hydrophobic type II receptor site of BMP-2. Superimposition of the Col2a vWC SD1 and CCN3 vWC SD1 with CV-2 vWC1 SD1 bound to BMP-2, demonstrates how the absence of the N-terminal clip and the extended loop in the first strand of SD1 prevents the same interaction with BMP-2 (Fig. 2*E*). Taken together, it is unlikely that Col2a vWC and CCN3 vWC can bind to BMP-2 in the same manner as CV-2 vWC1.

Characterisations of vWC:BMP-2 interactions– To support our structural analyses that suggest new modes of vWC:BMP-2 interactions, we set about characterising the binding of Col2a and CCN3 vWC domains to BMP-2 using surface plasmon resonance (SPR). Purified recombinant mature domain of BMP-2 was covalently immobilised on the surface of the sensor chip, and purified Col2a and CCN3 vWC domains were flowed over the sensor chip. As has been shown previously (19, 24), Col2a vWC was found to bind to BMP-2, albeit at low affinity. The binding rate constants k_{off} (7×10^{-3} s^{-1}) and k_{on} (7×10^2 $M^{-1}s^{-1}$) were determined by fitting kinetic data to a 1:1 binding model, resulting in a K_D of 10 μM ($K_D = k_{off}/k_{on}$) (Fig. 3*A*). This calculated binding affinity was validated by equilibrium SPR experiments, resulting in a K_D of 42 μM (Fig. 3*B*).

However, despite having a similar SD1 structure to Col2a vWC, CCN3 vWC did not show any detectable binding to BMP-2 at concentration range up to 40 μM when analysed by SPR in identical conditions used for Col2a vWC (Fig. 3*C*). Given that we use highly purified and homogenous protein, we are very confident that interaction between BMP-2 and CCN3 (and most likely other CCN proteins) is not mediated by the vWC domain, or, at most, its contribution to the binding is very small.

Based on these structural and biophysical data, it is clear that the residues responsible for BMP-2 binding in the Col2a vWC are unlikely to be the same as in CV-2 vWC1. Given that structurally more similar CCN3 vWC is not binding to BMP-2, the BMP-2 binding residues in Col2a would not be conserved in CCN3 either. To define the binding epitope of Col2a vWC to BMP-2, we identified two conserved clusters of surface-exposed hydrophobic residues: I. V46, I54, V56, L63, and I67 in SD1, and II. I80, F82, and I88 in SD2 (Fig. 4*A* and 5*A*). Site I in SD1 is in the opposite side to the CV-2 vWC1 epitope, whereas the site in the SD2 is directly below the CV-2 vWC1 epitope. We mutated these residues in pairs (based on closeness in the 3D structure) to alanines, generating four mutants of Col2a vWC (Fig. 4*A*). All the mutants were expressed and purified as the wild type domain, appearing to produce well-folded proteins.

The effect of these mutations on the interaction with BMP-2 was monitored by SPR. These SPR experiments revealed that all three mutants containing mutations in site I, V46A+I54A, V56A+L63A, and I67A+I80A, showed no interaction with BMP-2, whereas the F82A+I88A mutant, with both residues in site II, retained its ability to bind BMP-2 (Fig. 4*B-G*). Since the interaction between the Col2a vWC and BMP-2 is weak (K_D 10-42 μM), it is not surprising that mutation of one or two residues involved in the binding can be enough to completely disrupt the interaction. Taken together, it can be inferred that the binding epitope of Col2a vWC to BMP-2 resides in site I, on the opposite side of SD1 to the CV-2 vWC1 epitope, with residues V46 and/or I54, V56 and/or L63, and I67 contributing to the hydrophobic interactions with BMP-2.

DISCUSSION

We have determined the structures of the vWC domains of collagen IIA and CCN3 using X-ray crystallography. Through structural comparison with CV-2 vWC1, we predict that Col2a vWC and CCN3 vWC are not able to bind to BMP-2 in the same manner as CV-2 vWC1. Using SPR, we analysed the binding of the two vWC domains of collagen IIA and CCN3 to BMP-2. Kinetic rate constants of the Col2a vWC:BMP-2 interaction were measured, and the binding affinity was determined using both kinetic and equilibrium SPR data. CCN3 vWC, on the other hand, showed no

binding to BMP-2 at the same concentration range used as Col2a vWC. Leveraging our structural analysis, we identified the binding epitope of Col2a vWC to BMP-2 as a hydrophobic patch on the opposite side of SD1 as the previously characterised BMP-2 binding site in CV-2 vWC1.

Both Col2a and CCN3 vWC domains show a typical tripartite structure of an N-terminal region, and two subdomains SD1 and SD2. The non-globular, extended confirmation of the vWC domains potentially allows a great deal of flexibility for the relative orientation of SD2 to SD1, as has been observed in solution NMR structures of Col2a vWC and CV-2 vWC1 (17, 23). Given this flexibility, the hydrogen bond network between β-sheets in adjacent molecules in the asymmetric units of both Col2a and CCN3 vWCs must be key contributions to the well-diffracting crystals (Fig. S1*B* and S3*B*). As commonly observed in most cysteine-rich extracellular proteins, the formation of the disulfide bonds are largely responsible for the stability of this small domain, reflected in the complete conservation of these residues. One of the unique features that we observe in Col2a vWC and CCN3 vWC, but not in CV-2 vWC1, is the π-π interaction that locks the orientation of the N-terminal β-hairpin. The two aromatic residues that form this π-π interaction, one in the N-terminal region and the other in the SD1, are conserved in more than half (162 out of 259) of the vWC domains found in human proteins (Fig. S6), including vWC domains known to bind BMP-2 (Fig. 5*B*). These vWC domains would potentially share the N-terminal structure of the β-hairpin with Col2a vWC and CCN3 vWC, rather than the extended clip-like fold found in CV-2 vWC1.

The two major binding epitopes for BMP-2 in CV-2 vWC1, the N-terminal clip and the extended first strand in SD1, are both absent in our Col2a vWC and CCN3 vWC structures. It was suggested by Zhang *et al.* (18) that the Col2a vWC could undergo major conformational rearrangements to make the same epitope accessible for binding to BMP-2. However, a solution NMR structure of the CV-2 vWC1 in its unbound state showed that the conformations of both epitopes were pre-defined, with the angle of the N-terminal clip relative to SD1 being fixed and the extended first strand in SD1 being very rigid (23). Instead, our mutational study on Col2a vWC has uncovered a novel BMP-2 binding epitope on the opposite side of SD1 as

compared with that in the CV-2 vWC1. Sequence conservation analysis has also shown that this epitope is highly conserved across different species, with a score of 9 (9 to 1 from conserved to variable) for V46, V56, and L63, 8 for I54, and 7 for I67 (Fig. 5*A* and S7). Since the structure of the CCN3 vWC revealed no conservation of either of the two CV-2 vWC1 epitopes nor the residues involved in binding in Col2a vWC, it is not surprising that we did not observe any binding of CCN3 vWC to BMP-2. However, the association between the CCN family and the BMPs is clearly evident in the literature (25, 43–48), therefore this interaction must be mediated through one or more of the three other domains (IB, TSP1, or CTCK) in the CCN proteins.

This new mechanism of vWC:BMP interaction provides insights into the possible binding modes of other BMP-binding vWC domains (Table 2 and Fig. 5*B*). For Chordin and CHL2, their vWC1 and vWC3 were both shown to bind BMP-2 in the SD1 (22). Residues involved in the binding in CHL2 vWC1 and vWC3 were also identified by mutational analysis by Fujisawa *et al* (22). Sequence alignment with Col2a vWC and CV-2 vWC1 suggests that these residues lie in the first strand of SD1 (Fig. 5*B*), and given that CHL2 and Chordin possess 7-10 more residues in this region, it is possible that they form an even more extended loop towards the BMP-2 and share the same epitope with CV-2 vWC1. However, the two aromatic residues that form the π-π interaction between the N-terminal region and SD1 may make it conformationally more preferable to access BMP-2 from the opposite side as we have shown for the Col2a vWC. It is also possible that these vWC domains bind BMP-2 through yet another epitope, and further studies are necessary to parse this question.

Besides CV-2, previous studies have revealed inhibition mechanisms of other known antagonists of BMP signalling, typically through blocking the type I and type II receptor binding sites. Similar to CV-2, both Noggin and Gremlin-2 utilise their flexible and extended N-terminal regions to reach into the type I receptor binding site of BMP, together with additional interfaces that overlap with the type II receptor site (11, 14). Gremlin-1 also shares the binding sites of both type I and II receptors, although not involving its N-termini (12). Despite similar inhibition mechanisms, the stoichiometries of these antagonists with their

ligand BMPs are quite diverse. One dimeric Noggin binds to one dimeric BMP with a 1:1 stoichiometry, whereas two molecules of CV-2 vWC1 bind to each protomer of a dimeric BMP with a 2:1 stoichiometry. For Gremlin-1 and -2, distinguished features of elongated fibrils of oligomeric complexes have been suggested, where each protomer of a dimeric Gremlin binds to one protomer of BMP, forming an alternating, open-ended oligomer (12, 14). To elucidate the binding mechanism by Col2a, future studies should include mutagenesis of receptor binding sites on BMP-2, complex crystallisation, and small-angle X-ray scattering analysis.

The affinity of Col2a vWC for BMP-2 we obtained is much lower when comparing with the vWC domains in CV-2, Chordin and CHL2 (Table 2). However, the affinity of full-length Chordin and CHL2, which allows multiple vWC domains to simultaneously bind BMP-2, is 7.5-2500 fold higher than their individual vWC domains (Table 2) (18, 21, 22, 49). *In vivo*, collagen molecules self-associate into trimeric coils and to further oligomeric fibrils, with the vWC domain containing N-terminal propeptide accessible on the surface of the collagen fibrils (24). Multimeric collagen could allow two vWC domains to interact simultaneously with a dimeric BMP-2, forming oligomeric fibrils like the Gremlins (12, 14), and thereby increase the apparent affinity between the two proteins due to avidity effects. In fact, Col2a vWC expressed as a GST fusion protein has been shown to bind BMP-2 with nanomolar affinity (24). Furthermore, previous studies with *Xenopus laevis* oocytes demonstrated anti-BMP-2 activity with full-length collagen IIA but not with isolated Col2a vWC domain (19), suggesting that avidity effects play a significant role in the biological efficacy of Col2a vWC. BMPs are also thought to bind to fibrillar collagen directly and such interactions could exist alongside vWC binding, and further stabilise such complex. Furthermore, like all TGF-β family growth factors, BMPs are synthesised as larger precursors and the pro-peptides can interact with components of the extracellular matrix (50). Col2a vWC interaction is therefore one of the many ways BMPs interact with ECM.

As collagen is a major structural component of the extracellular matrix, its binding of BMP-2 could affect the localisation and generation of morphogenetic gradients during development.

Procollagen IIA is expressed in epithelial and mesenchymal cells prior to differentiation, suggesting it may play an important role in tissue differentiation and body patterning (26–28). In our biological activity assays, we did not observe inhibition or stimulation of the BMP-2 signalling by monomeric Col2a vWC (data not shown). This could be due to the low affinity binding by a single vWC domain rather than the trimeric full-length collagen. Alternatively, the binding to BMP-2 by collagen could be neutral with regards to BMP-2 bioactivity, with collagen instead serving as a scaffold for localisation and storage of BMP-2, assisting in its gradient formation and presenting it to other extracellular regulators. While we have not been able to characterise the BMP-2:Col2a vWC complex structurally, our data suggest distinct mode of interaction that has been observed with CV-2 and noggin. Localisation of the BMP-2-binding epitope on the relatively flat surface of the Col2a vWC domain suggests that this interaction cannot involve both the type I and II receptor binding sites, which are located on the opposite sides of the growth factor.

EXPERIMENTAL PROCEDURES

Cloning, Expression, and Purification–Human collagen IIA vWC domain (residues 31-98, Uniprot P02458) and rat CCN3 vWC domain (residues 100-195, Uniprot Q9QZQ5) were expressed in BL21(DE3) *E. coli* using the pHAT3 and pBAT4 vectors (51), respectively. DNA for the Col2a vWC construct was codon optimised for *E. coli* and synthesised by PCR using overlapping oligonucleotides (all oligonucleotide sequences are listed in the Supplementary material). CCN3 was amplified from cDNA (kind gift from Dr Paul Kemp). vWC mutants were generated by a two-step PCR protocol using overlapping oligonucleotide across the mutated regions and cloned into expression vectors as the wild type proteins. All constructs were confirmed by dideoxy sequencing. For protein expression, *E. coli* BL21(DE3) competent cells of were transformed with the expression plasmid and grown on L-agar plates in the presence of 100 μg/ml of ampicillin overnight. The following day, cells from the plate were cultured in 2-YT medium with 100 μg/ml ampicillin at 37 °C under agitation. Cells were induced with 400 μM isopropyl-β-D-

thiogalactoside at an OD_{600nm} of 0.8 and left to express the proteins for 4 h. Both proteins were expressed solubly, despite the presence of 10 cysteines that form disulfide bridges in the folded proteins.

His-tagged Col2a vWC was purified by Ni-NTA affinity chromatography, followed by cleavage of the His-tag by thrombin protease, and final purification by reversed phase chromatography (ACE® 5 C8-300). CCN3 vWC was purified by anion exchange (HiTrap™ Q HP, GE Healthcare) and size exclusion chromatographies (HiLoad™ 16/60 Superdex™ 75, GE Healthcare) followed by reversed phase chromatography (ACE® 5 C8-300). Both proteins were lyophilised and resuspended in water after reverse phase chromatography. Purified proteins were analysed by MALDI mass spectrometry and were observed to have the mass for proteins in which all cysteine residues have been oxidised to cystines. In order to obtain experimental phases for CCN3 vWC crystal structure determination, the V105M/R128M mutant protein was labelled with selenomethionine using the metabolic suppression method and purified like the wild type domain.

Production of BMP-2 has been described previously (12).

Crystallisation and structure determination– Crystals of the SeMet-labelled CCN3 vWC mutant grew in 3.4 M NaCl, 100 mM MES pH 6.8, in 1 µl + 1µl drops. Crystals were cryoprotected with 10% glycerol and cryocooled in liquid nitrogen. Data from these crystals were collected at ESRF beamline BM14 at Selenium peak at a wavelength of 0.97963 Å. Data were processed using XDS and the experimental phases were derived from the SAD data using autoSHARP (52). The initial model was built automatically using ARP/wARP (53). Crystals of unlabelled CCN3 vWC domain grew in 0.8 M K/Na tartrate, 0.4 M NaCl, 0.1 M imidazole pH 8.0. The crystals were cryo-protected in 30 % glycerol and cryo-cooled in liquid nitrogen. X-ray diffraction data were collected at Diamond Light Source, beamline I04-1, using a Pilatus 2M detector (Dectris, Switzerland), at wavelength 0.9173 Å. X-ray diffraction data of CCN3 vWC were indexed, integrated, and scaled using XDS (54). Two datasets obtained from separate crystals were merged using XSCALE (54). Molecular replacement was performed by AMoRe (55), using the experimentally phased CCN3 vWC

V105M/R128M mutant structure as the search model. Refinement was performed using Refmac 5.5 (56) and Phenix 1.8.4 (57). Coot (58) was used for iterative model building and initial validation.

Col2a vWC domain was crystallised by mixing 1 uL protein at a concentration of 10 mg/mL and 1 uL reservoir solution (0.1 M HEPES, pH 7.5, 40% PEG 200) in a sitting drop vapour diffusion setup. Experimental phases were obtained from sulphur single wavelength anomalous dispersion (SAD). Anomalous data were collected at a wavelength of 1.9 Å at beamline I04 of Diamond Light Source and processed via autoPROC (59). Phases were obtained using ShelxC, ShelxD, and ShelxE (60) through the HKL2MAP (61) interface. An initial model was obtained through automated model building using Buccaneer (62). Further iterative model building was performed using autoBUSTER (63) and Coot (58). This preliminary model was then used in molecular replacement (PHASER (64)) to extend the resolution to data collected at a wavelength of 0.9686 Å at beamline I24 at Diamond Light Source and refined as above.

Statistics of X-ray data collection and structure refinement are shown in Table 1. Both Col2a and CCN3 vWC structures have been deposited in the Protein Data Bank with accession codes 5NIR and 5NB8, respectively.

Conservation analysis–The degree of evolutionary conservation of the amino acids in the Col2a vWC and CCN3 vWC domains was analysed using the ConSurf server (http://consurf.tau.ac.il/) (65), in order to reveal the regions that are important for the function and/or structure of the protein. Sequences of Col2a vWC and CCN3 vWC across species were extracted from the *Ensembl* database (release 86, http://www.ensembl.org/index.html), aligned and scored for position-specific conservation by the ConSurf Server, and mapped onto the surfaces of the corresponding structures (65).

Surface plasmon resonance (SPR)–SPR binding assays were performed on a BIAcore T100 instrument (GE Healthcare). HBS-EP+ buffer (20 mM HEPES, 150 mM NaCl, 3 mM EDTA, 0.05% (v/v) Surfactant P20, pH 7.4) with the addition of 1 mg/ml CM-Dextran salt was used as the running buffer at a flow rate of 30 µl/min. BMP-2 (residues 283-396) was directly immobilised on a CM5 sensor chip (GE Healthcare) *via* amine coupling. Wild-type and mutants of Col2a vWC, as well as

the CCN3 vWC, were used as analytes. The surface was regenerated with 4 M guanidinium chloride. The sensograms were corrected for unspecific binding by subtracting the signal from the reference channel. Data were analysed with BIAcore T100 Evaluation Software 2.0.3 (GE Healthcare) and proFit (QuantumSoft) using kinetic and equilibrium equations for a 1:1 interaction.

ACKNOWLEDGEMENTS

CONFLICT OF INTEREST
The authors declare that they have no conflicts of interest with the contents of this article.

AUTHOR CONTRIBUTIONS
MH conceived and coordinated the study and E-RX, EEB, and MH designed the experiments. EEB performed the experiments with Col2a vWC domain, E-RX performed the experiments with CCN3 vWC domain and Col2a vWC mutants. GF determined the structure of Col2a vWC domain, MH determined the original CCN3 vWC domain. All authors analysed the results, wrote, revised, and approved the final version of the manuscript. E-RX and EEB contributed equally and are equal first authors.

FOOTNOTES
The abbreviations used are: BMP, bone morphogenetic protein; vWC, von Willebrand factor C domain; Col2a, collagen type IIα; CV-2, Crossveinless-2; CHL2, Chordin-like 2; Nov, Nephroblastoma overexpressed; SPR, surface plasmon resonance

REFERENCES
1.   Hogan, B. L. M. (1996) Bone morphogenetic proteins in development. *Curr. Opin. Genet. Dev.* **6**, 432–438

2.   Reddi, A. (2003) Cartilage morphogenetic proteins: role in joint development, homoeostasis, and regeneration. *Ann. Rheum. Dis.* **62**, ii73-ii78

3.   Simic, P., and Vukicevic, S. (2005) Bone morphogenetic proteins in development and homeostasis of kidney. *Cytokine Growth Factor Rev.* **16**, 299–308

4.   Moura, J., Da Silva, L., Cruz, M. T., and Carvalho, E. (2013) Molecular and cellular mechanisms of bone morphogenetic proteins and activins in the skin: Potential benefits for wound healing. *Arch. Dermatol. Res.* **305**, 557–569

5.   Tobin, J. F., and Celeste, A. J. (2006) Bone morphogenetic proteins and growth differentiation factors as drug targets in cardiovascular and metabolic disease. *Drug Discov. Today*. **11**, 405–411

6.   Manson, S. R., Song, J. B., Guo, Q., Liapis, H., and Austin, P. F. (2015) Cell type specific changes in BMP-7 expression contribute to the progression of kidney disease in patients with obstructive uropathy. *J. Urol.* **193**, 1860–1869

7.   Cai, J., Pardali, E., Sánchez-Duffhues, G., and Ten Dijke, P. (2012) BMP signaling in vascular

diseases. *FEBS Lett.* **586**, 1993–2002

8.   Bandyopadhyay, A., Yadav, P. S., and Prashar, P. (2013) BMP signaling in development and diseases: A pharmacological perspective. *Biochem. Pharmacol.* **85**, 857–864

9.   Miyazono, K., Kamiya, Y., and Morikawa, M. (2010) Bone morphogenetic protein receptors and signal transduction. *J. Biochem.* **147**, 35–51

10.   Balemans, W., and Van Hul, W. (2002) Extracellular regulation of BMP signaling in vertebrates: A cocktail of modulators. *Dev. Biol.* **250**, 231–250

11.   Groppe, J., Greenwald, J., Wiater, E., Rodriguez-Leon, J., Economides, A. N., Kwiatkowski, W., Affolter, M., Vale, W. W., Belmonte, J. C. I., and Choe, S. (2002) Structural basis of BMP signalling inhibition by the cystine knot protein Noggin. *Nature*. **420**, 636–642

12.   Kišonaitė, M., Wang, X., and Hyvönen, M. (2016) Structure of Gremlin-1 and analysis of its interaction with BMP-2. *Biochem. J.* **473**, 1593–604

13.   Salazar, V. S., Gamer, L. W., and Rosen, V. (2016) BMP signalling in skeletal development, disease and repair. *Nat. Rev. Endocrinol.* **12**, 203–221

14.   Nolan, K., Kattamuri, C., Rankin, S. A., Read, R. J., Zorn, A. M., and Thompson, T. B. (2016) Structure of Gremlin-2 in Complex with GDF5 Gives Insight into DAN-Family-Mediated BMP Antagonism. *Cell Rep.* **16**, 2077–2086

15.   Nolan, K., Kattamuri, C., Luedeke, D. M., Deng, X., Jagpal, A., Zhang, F., Linhardt, R. J., Kenny, A. P., Zorn, A. M., and Thompson, T. B. (2013) Structure of protein related to DAN and Cerberus: Insights into the mechanism of bone morphogenetic protein antagonism. *Structure*. **21**, 1417–1429

16.   Mancuso, D. J., Tuley, E. A., Westfield, L. a, Worrall, N. K., Shelton-Inloes, B. B., Sorace, J. M., Alevy, Y. G., and Sadler, J. E. (1989) Structure of the gene for human von Willebrand factor. *J. Biol. Chemystry*. **264**, 19514–19527

17.   O'Leary, J. M., Hamilton, J. U., Deane, C. M., Valeyev, N. V., Sandell, L. J., and Downing, A. K. (2004) Solution structure and dynamics of a prototypical chordin-like cysteine-rich repeat (von Willebrand factor type C module) from collagen IIA. *J. Biol. Chem.* **279**, 53857–53866

18.   Zhang, J. li, Qiu, L. yan, Kotzsch, A., Weidauer, S., Patterson, L., Hammerschmidt, M., Sebald, W., and Mueller, T. D. (2008) Crystal Structure Analysis Reveals How the Chordin Family Member Crossveinless 2 Blocks BMP-2 Receptor Binding. *Dev. Cell*. **14**, 739–750

19.   Larraín, J., Bachiller, D., Lu, B., Agius, E., Piccolo, and Robertis, D. (2000) BMP-binding modules in chordin: a model for signalling regulation in the extracellular space. *Development*. **127**, 821–830

20.   Garcia Abreu, J., Coffinier, C., Larraín, J., Oelgeschläger, M., and De Robertis, E. M. (2002) Chordin-like CR domains and the regulation of evolutionarily conserved extracellular signaling systems. *Gene*. **287**, 39–47

21.   Zhang, J.-L., Huang, Y., Qiu, L.-Y., Nickel, J., and Sebald, W. (2007) von Willebrand factor type C domain-containing proteins regulate bone morphogenetic protein signaling through different recognition mechanisms. *J. Biol. Chem.* **282**, 20002–20014

22.   Fujisawa, T., Huang, Y., Sebald, W., and Zhang, J. L. (2009) The binding of von Willebrand factor type C domains of Chordin family proteins to BMP-2 and Tsg is mediated by their SD1 subdomain. *Biochem. Biophys. Res. Commun.* **385**, 215–219

23.   Fiebig, J. E., Weidauer, S. E., Qiu, L. Y., Bauer, M., Schmieder, P., Beerbaum, M., Zhang, J. L., Oschkinat, H., Sebald, W., and Mueller, T. D. (2013) The clip-segment of the von Willebrand domain 1 of the BMP modulator protein crossveinless 2 is preformed. *Molecules*. **18**, 11658–

11682

24. Zhu, Y., Oganesian, A., Keene, D. R., and Sandell, L. J. (1999) Type IIA Procollagen Containing the Cysteine-rich Amino Propeptide Is Deposited in the Extracellular Matrix of Prechondrogenic. *J. Cell Biol.* **144**, 1069–1080

25. Minamizato, T., Sakamoto, K., Liu, T., Kokubo, H., Katsube, K. ichi, Perbal, B., Nakamura, S., and Yamaguchi, A. (2007) CCN3/NOV inhibits BMP-2-induced osteoblast differentiation by interacting with BMP and Notch signaling pathways. *Biochem. Biophys. Res. Commun.* **354**, 567–573

26. Ryan, M. C., and Sandell, L. J. (1990) Differential expression of a cysteine-rich domain in the amino-terminal propeptide of type II (cartilage) procollagen by alternative splicing of mRNA. *J. Biol. Chem.* **265**, 10334–10339

27. Sandell, L. J., Nalin, A. M., and Reife, R. A. (1994) Alternative splice form of type II procollagen mRNA (IIA) is predominant in skeletal precursors and non-cartilaginous tissues during early mouse development. *Dev. Dyn.* **199**, 129–140

28. Oganesian, A., Zhu, Y., and Sandell, L. J. (1997) Type IIA Procollagen Amino Propeptide Is Localized in Human Embryonic Tissues. *J. Histochem. Cytochem.* **45**, 1469–1480

29. Williams, M. J., Phan, I., Harvey, T. S., Rostagno, A., Gold, L. I., and Campbell, I. D. (1994) Solution structure of a pair of fibronectin type 1 modules with fibrin binding activity. *J. Mol. Biol.* **235**, 1302–1311

30. Leask, A., and Abraham, D. J. (2006) All in the CCN family: essential matricellular signaling modulators emerge from the bunker. *J. Cell Sci.* **119**, 4803–4810

31. Lin, C. G., Leu, S. J., Chen, N., Tebeau, C. M., Lin, S. X., Yeung, C. Y., and Lau, L. F. (2003) CCN3 (NOV) is a novel angiogenic regulator of the CCN protein family. *J. Biol. Chem.* **278**, 24200–24208

32. Bleau, A. M., Planque, N., Lazar, N., Zambelli, D., Ori, A., Quan, T., Fisher, G., Scotlandi, K., and Perbal, B. (2007) Antiproliferative activity of CCN3: Involvement of the C-terminal module and post-translational regulation. *J. Cell. Biochem.* **101**, 1475–1491

33. Rydziel, S., Stadmeyer, L., Zanotti, S., Durant, D., Smerdel-Ramoya, A., and Canalis, E. (2007) Nephroblastoma overexpressed (Nov) inhibits osteoblastogenesis and causes osteopenia. *J. Biol. Chem.* **282**, 19762–19772

34. Janune, D., Kubota, S., Nishida, T., Kawaki, H., Perbal, B., Iida, S., and Takigawa, M. (2011) Novel effects of CCN3 that may direct the differentiation of chondrocytes. *FEBS Lett.* **585**, 3033–3040

35. Abd El Kader, T., Kubota, S., Janune, D., Nishida, T., Hattori, T., Aoyama, E., Perbal, B., Kuboki, T., and Takigawa, M. (2013) Anti-fibrotic effect of CCN3 accompanied by altered gene expression profile of the CCN family. *J. Cell Commun. Signal.* **7**, 11–18

36. Ohgawara, T., Kubota, S., Kawaki, H., Kurio, N., Abd El Kader, T., Hoshijima, M., Janune, D., Shimo, T., Perbal, B., Sasaki, A., and Takigawa, M. (2011) Association of the metastatic phenotype with CCN family members among breast and oral cancer cells. *J. Cell Commun. Signal.* **5**, 291–299

37. Cui, L., Xie, R., Dang, S., Zhang, Q., Mao, S., Chen, J., Qu, J., and Zhang, J. (2014) NOV promoted the growth and migration of pancreatic cancer cells. *Tumor Biol.* **35**, 3195–3201

38. McCallum, L., Price, S., Planque, N., Perbal, B., Pierce, A., Whetton, A. D., and Irvine, A. E. (2006) A novel mechanism for BCR-ABL action: Stimulated secretion of CCN3 is involved in growth and differentiation regulation. *Blood*. **108**, 1716–1723

39. Ouellet, V., and Siegel, P. M. (2012) CCN3 modulates bone turnover and is a novel regulator of skeletal metastasis. *J. Cell Commun. Signal.* **6**, 73–85

40. Chang, C. C., Lin, B. R., Wu, T. S., Jeng, Y. M., and Kuo, M. L. (2014) Input of microenvironmental regulation on colorectal cancer: Role of the CCN family. *World J. Gastroenterol.* **20**, 6826–6831

41. Bork, P. (1993) The modular architecture of a new family of growth regulators related to connective tissue growth factor. *FEBS Lett*. **327**, 125–130

42. Kawaki, H., Kubota, S., Suzuki, A., Suzuki, M., Kohsaka, K., Hoshi, K., Fujii, T., Lazar, N., Ohgawara, T., Maeda, T., Perbal, B., Takano-Yamamoto, T., and Takigawa, M. (2011) Differential roles of CCN family proteins during osteoblast differentiation: Involvement of Smad and MAPK signaling pathways. *Bone*. **49**, 975–989

43. Abreu, J. G., Ketpura, N. I., Reversade, B., and De Robertis, E. M. (2002) Connective-tissue growth factor (CTGF) modulates cell signalling by BMP and TGF-beta. *Nat. Cell Biol.* **4**, 599–604

44. Nakamura, Y., Weidinger, G., Liang, J. O., Aquilina-Beck, A., Tamai, K., Moon, R. T., and Warman, M. L. (2007) The CCN family member Wisp3, mutant in progressive pseudorheumatoid dysplasia, modulates BMP and Wnt signaling. *J. Clin. Invest.* **117**, 3075–3086

45. Nguyen, T. Q., Roestenberg, P., van Nieuwenhoven, F. A., Bovenschen, N., Li, Z., Xu, L., Oliver, N., Aten, J., Joles, J. A., Vial, C., Brandan, E., Lyons, K. M., and Goldschmeding, R. (2008) CTGF inhibits BMP-7 signaling in diabetic nephropathy. *J. Am. Soc. Nephrol.* **19**, 2098–2107

46. Maeda, A., Nishida, T., Aoyama, E., Kubota, S., Lyons, K. M., Kuboki, T., and Takigawa, M. (2009) CCN family 2/connective tissue growth factor modulates BMP signalling as a signal conductor, which action regulates the proliferation and differentiation of chondrocytes. *J. Biochem.* **145**, 207–216

47. Ono, M., Inkson, C. A., Kilts, T. M., and Young, M. F. (2011) WISP-1/CCN4 regulates osteogenesis by enhancing BMP-2 activity. *J. Bone Miner. Res.* **26**, 193–208

48. Pal, A., Huang, W., Li, X., Toy, K. A., Nikolovska-Coleska, Z., and Kleer, C. G. (2012) CCN6 modulates BMP signaling via the Smad-independent TAK1/p38 pathway, acting to suppress metastasis of breast cancer. *Cancer Res.* **72**, 4818–4828

49. Troilo, H., Zuk, A. V, Tunnicliffe, R. B., Wohl, A. P., Berry, R., Collins, R. F., Jowitt, T. A., Sengle, G., and Baldock, C. (2014) Nanoscale structure of the BMP antagonist chordin supports cooperative BMP binding. *Proc. Natl. Acad. Sci. U. S. A.* **111**, 13063–13068

50. Wohl, A. P., Troilo, H., Collins, R. F., Baldock, C., and Sengle, G. (2016) Extracellular regulation of bone morphogenetic protein activity by the microfibril component fibrillin-1. *J. Biol. Chem.* **291**, 12732–12746

51. Peränen, J., Rikkonen, M., Hyvönen, M., and Kääriäinen, L. (1996) T7 vectors with modified T7lac promoter for expression of proteins in Escherichia coli. *Anal. Biochem.* **236**, 371–373

52. Bricogne, G., Vonrhein, C., Flensburg, C., Schiltz, M., and Paciorek, W. (2003) Generation, representation and flow of phase information in structure determination: Recent developments in and around SHARP 2.0. *Acta Crystallogr. - Sect. D Biol. Crystallogr.* **59**, 2023–2030

53. Langer, G., Cohen, S. X., Lamzin, V. S., and Perrakis, A. (2008) Automated macromolecular model building for X-ray crystallography using ARP/wARP version 7. *Nat. Protoc.* **3**, 1171–1179

54. Kabsch, W. (2010) Xds. *Acta Crystallogr. Sect. D Biol. Crystallogr.* **66**, 125–132

55. Navaza, J. (1994) AMoRe: an automated package for molecular replacement. *Acta Crystallogr. Sect. A*. **50**, 157–163

56.   Vagin, A. A., Steiner, R. A., Lebedev, A. A., Potterton, L., McNicholas, S., Long, F., and Murshudov, G. N. (2004) REFMAC5 dictionary: Organization of prior chemical knowledge and guidelines for its use. *Acta Crystallogr. Sect. D Biol. Crystallogr.* **60**, 2184–2195

57.   Adams, P. D., Afonine, P. V., Bunkóczi, G., Chen, V. B., Davis, I. W., Echols, N., Headd, J. J., Hung, L. W., Kapral, G. J., Grosse-Kunstleve, R. W., McCoy, A. J., Moriarty, N. W., Oeffner, R., Read, R. J., Richardson, D. C., Richardson, J. S., Terwilliger, T. C., and Zwart, P. H. (2010) PHENIX: A comprehensive Python-based system for macromolecular structure solution. *Acta Crystallogr. Sect. D Biol. Crystallogr.* **66**, 213–221

58.   Emsley, P., and Cowtan, K. (2004) Coot: Model-building tools for molecular graphics. *Acta Crystallogr. Sect. D Biol. Crystallogr.* **60**, 2126–2132

59.   Vonrhein, C., Flensburg, C., Keller, P., Sharff, A., Smart, O., Paciorek, W., Womack, T., and Bricogne, G. (2011) Data processing and analysis with the autoPROC toolbox. *Acta Crystallogr. Sect. D Biol. Crystallogr.* **67**, 293–302

60.   Sheldrick, G. M. (2007) A short history of SHELX. *Acta Crystallogr. Sect. A Found. Crystallogr.* **64**, 112–122

61.   Pape, T., and Schneider, T. R. (2004) HKL2MAP : a graphical user interface for macromolecular phasing with SHELX programs. *J. Appl. Crystallogr.* **37**, 843–844

62.   Cowtan, K. (2006) The Buccaneer software for automated model building. 1. Tracing protein chains. *Acta Crystallogr. Sect. D Biol. Crystallogr.* **62**, 1002–1011

63.   Bricogne G., Blanc E., Brandl M., Flensburg C., Keller P., P. W., and Roversi P, Sharff A., Smart O.S., Vonrhein C., W. T. O. (2016) BUSTER version 2.11.5. *Cambridge, United Kingdom Glob. Phasing Ltd.*

64.   McCoy, A. J., Grosse-Kunstleve, R. W., Adams, P. D., Winn, M. D., Storoni, L. C., and Read, R. J. (2007) Phaser crystallographic software. *J. Appl. Crystallogr.* **40**, 658–674

65.   Ashkenazy, H., Abadi, S., Martz, E., Chay, O., Mayrose, I., Pupko, T., and Ben-Tal, N. (2016) ConSurf 2016: an improved methodology to estimate and visualize evolutionary conservation in macromolecules. *Nucleic Acids Res.* **44**, 1–7

FIGURE LEGENDS

FIGURE 1. The tripartite structure of the vWC domains of Col2a and CCN3. *A*, Domain diagrams of Col2a and CCN3 with the two vWC domains coloured in *purple* and *red*, respectively. The bars underneath the diagrams indicate the parts of the proteins used in this study. *B,* Ribbon diagram of the crystal structure of Col2a vWC, with insets showing 90° rotated detailed views of each of the three major structural features with start and end residues labelled. Disulfide bonds are labelled and shown in *yellow*, and key π-π aromatic residues are labelled and shown in *teal*. The disulfide connectivity is show schematically at the bottom of the panel with the residue numbers of each cysteine underneath the diagram. *C,* Comparison of the novel crystal structure with the existing NMR ensemble of Col2a vWC (PDB entry 1U5M, thin *grey* lines), aligned based on the structures of the β-hairpin and SD1. *D,* Ribbon diagram of the CCN3 vWC with insets showing 90° rotated views of each of the three major structural features with the start and end residues labelled. Disulfide bonds are labelled and shown in *yellow*, and key π-π aromatic residues are labelled and shown in *teal*. The disulfide connectivity is show schematically at the bottom of the panel, as in (*B*).

FIGURE 2. Structural and BMP-2 binding epitope comparisons among vWC domains. *A-C*, Overlays of the Col2a *(purple)* and CCN3 (*red*), Col2a (*purple*) and CV-2 (*turquoise,* PDB entry 3BK3*)*, and CCN3 (*red*) and CV-2 (*turquoise*) vWCs, respectively, with insets showing 90° rotated views of each of the three major structural features. *D,* Overlay of the three vWC domains, with a zoomed in inset highlighting the disulfide bonds that link SD1 and SD2. *E*, Structure of BMP-2 (*grey* with semi-transparent surface) in complex with vWC domain from CV-1 (*turquoise*). The insets show overlays of Col2a vWC SD1 and CCN3 vWC SD1 with CV-2 vWC1 SD1 bound to BMP-2 (*grey*). Residues in CV-2 involved in BMP-2 binding are shown as sticks.

FIGURE 3. Characterisation of the binding of Col2a and CCN3 vWC domains to immobilised BMP-2 by SPR analysis. *A*, Kinetic analysis of Col2a vWC binding to BMP-2. BMP-2 was immobilised while 10 – 250 μM Col2a vWC was flowed over the sensor chip surface. Raw data is shown in *light gray* with fitting curves overlaid in *black*. Each dissociation and association phase was fit separately to give a k_{on} of 700 ± 300 M^{-1}s^{-1}, k_{off} of $7\times10^{-3} \pm 3\times10^{-3}$ s^{-1}, and K_D (k_{off}/k_{on}) of 11 μM (n=2). *B,* Equilibrium binding of Col2a vWC to BMP-2. Equilibrium response was plotted as dose dependency of Col2a vWC and fit to give a K_D of 42 ± 6 μM (n=2). Raw traces are shown as inset. *C,* Binding of 40 μM Col2a vWC and CCN3 to BMP-2 are shown as indicated in the graph.

FIGURE 4. Mutational analysis of the BMP-2 binding epitope of Col2a vWC. *A*, Ribbon diagram of the Col2a vWC crystal structure showing surface exposed hydrophobic residues selected for mutagenesis in site I and II. *B-G*, binding of Col2a vWC variants to immobilised BMP by SPR analysis. *B*, SPR sensorgrams of 40 μM wild-type (*black*) and mutants (coloured as in *A*) of Col2a vWC binding to BMP-2. *C-G,* SPR sensorgrams of increasing concentrations of Col2a vWC variants (coloured as in *A* and *B*), ranging from 10 nM to 50 μM sequentially injected at the time points indicated by arrows.

FIGURE 5. Conservation of Col2a vWC structural and binding motifs. *A,* Conservation of amino acid residues of Col2a among species is shown pictorially using the ConSurf server (http://consurf.tau.ac.il/) (65). Residues selected for our mutational analysis are labelled. Full sequence alignments are shown in Figure S7. *B*, Sequence alignment of vWC SD1s known to bind BMP-2. Col2a (human, Uniprot P02458), CV-2 (zebrafish, Q5D734), Chordin (mouse, Q9Z0E2) and CHL2 (mouse, Q8VEA6) were aligned using Clustal Omega. Conserved cysteines are highlighted in *yellow*, and conserved π-π aromatic residues in *teal*. Residues involved in Col2a binding to BMP-2 identified in this study are highlighted in *purple*. Residues previously shown to be involved in vWC binding to BMP-2 are highlighted in *pink* (18, 22).

Table 1. X-ray data collection and refinement statistics.

	Col2a vWC		CCN3 vWC	CCN3 vWC V105M/R128M
PDB code	5NIR	n/a	5NB8	n/a
Data collection				
Temperature (K)	100	100	100	100
Beamline	DLS I24	DLS I02	DLS I04-1	ESRF BM14
Wavelength (Å)	0.9686	1.9000	0.9173	0.9793
Space group	$P2_12_12_1$	$P2_12_12_1$	P1	C2
Cell dimensions				
a, b, c (Å)	31.9, 60.2, 86.4	30.1, 59.6, 86.6	38.4, 43.1, 72.3	141.7, 43.4, 38.0
α, β, γ (°)	90.0, 90.0, 90.0	90.0, 90.0, 90.0	75.3, 2.0, 89.9	90.0, 98.0, 90.0
Resolution (Å)	49.37-1.74 (1.75-1.74)	59.58-1.84 (1.85-1.84)	28.58-2.10 (2.20-2.10)	19.01-2.43 (2.59-2.43)
R_{merge}[b]	0.042 (0.709)	0.053 (0.560)	0.083 (0.596)	0.068 (0.269)
$<I> / \sigma<I>$	22.7 (2.2)	24.8 (2.2)	10.94 (2.60)	12.04 (4.35)
Number of reflections	112750	144119	130125	65573
CC ½	1.00 (0.898)	0.999 (0.886)	0.998 (0.864)	0.997 (0.936)
Unique reflections	17667	12829	25475	16452
Multiplicity	6.4 (5.9)	11.2 (6.7)	5.1 (4.7)	4.0 (4.0)
Completeness (%)	100.0 (100.0)	90.8 (37.2)	98.1 (95.3)	97.2 (96.3)
Refinement				
Resolution (Å)	49.37-1.74 (1.84-1.74)		28.58-2.10 (2.18-2.10)	
No. reflections/free	17616 / 894		25446 / 1298	
R_{work} / R_{free}	0.210 / 0.231 (0.222 / 0.257)		0.189 / 0.216 (0.253 / 0.302)	
No. atoms				
Protein	1010		2149	
Ligand/ion	207		31	
Water	16		155	
B-factors(Å^2)				
Protein	35.3		49.8	
Ligand/ion	48.8		92.7	
Water	47.2		50.5	
R.m.s. deviations				
Bond lengths (Å)	0.01		0.007	
Bond angles (°)	1.18		0.872	

Values in parentheses are for the highest-resolution shell.

Table 2. BMP-2 binding affinities of full-length and/or vWC domains of Col2a, CV-2, Chordin, and CHL2.

	Col2a	CV-2		Chordin				CHL2		
	vWC	Full	vWC1	Full	vWC1	vWC3	vWC4	Full	vWC1	vWC3
K_D (nM)	42000	22[21]	22[21] 20[18]	20[21]	150[21] 900[22]	900[21] 1050[22]	50000[21]	10[21]	2200[21] 1000[22]	300[21] 300[22]

Figure 1.
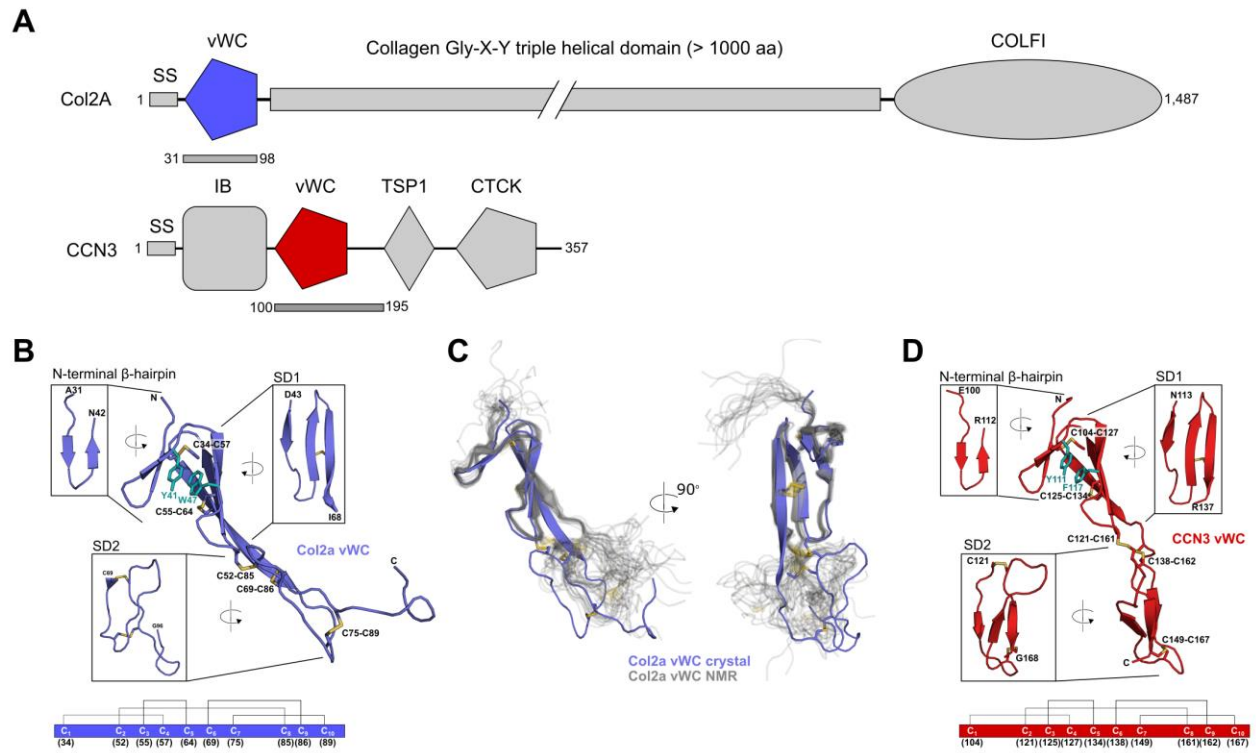
Figure 2.
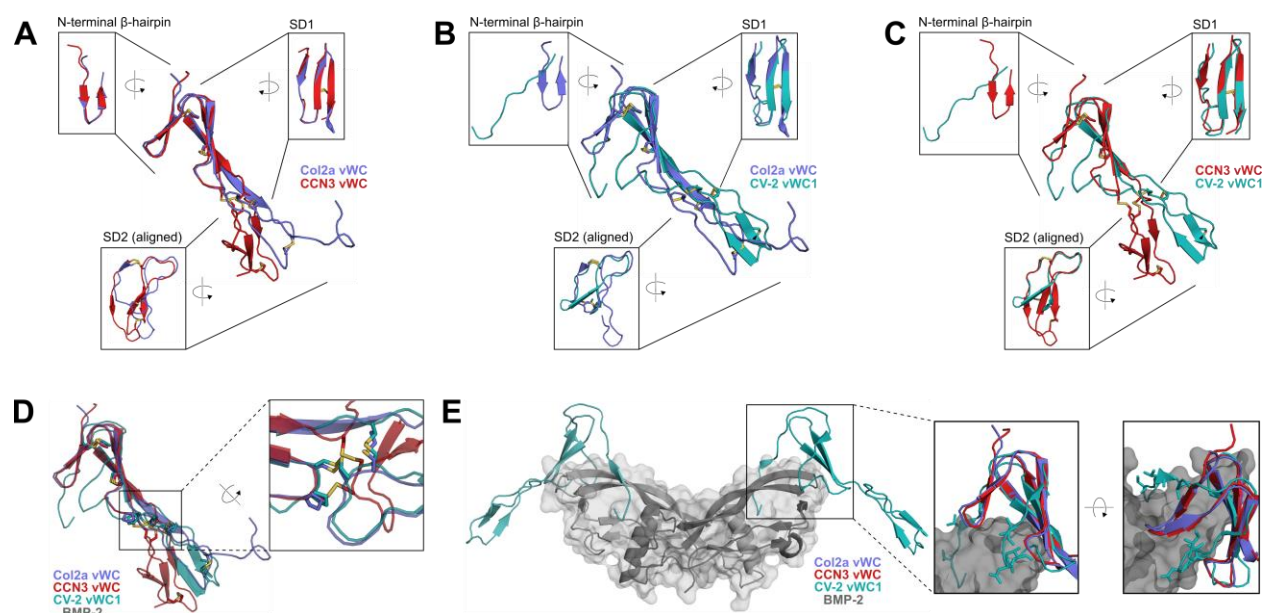
Figure 3.

Figure 4.

Figure 5.

A

L63
V56
I67
I54
V46
I88
F82

F82
I80
L63

| 1 | 2 | 3 | 4 | 5 | 6 | 7 | 8 | 9 |

Variable   Average   Conserved

B

```
Col2a vWC (34-68)      CVQDG-QRY-NDKDVWKP--------EPCRICVCDT----------GTVLCDDII--
CV-2 vWC1 (36-69)      CENEG--------EVLHI---PNITDNPCISCVCLNQ----------KAECKQEK--
Chordin vWC1 (51-105)  CSFGG-KVY-ALDETWHPDLGEPFGVMRCVLCACEAPQWARRGRGPGRVSCKNIKPQ
Chordin vWC3 (779-824) CYFDGDRSWRAAGTRWHPVV-PPFGLIKCAVCTCKGAT--------GEVHCEKVQ--
Chordin vWC4 (876-917) CRFAG-QWF-PENQSWHPSV-PPFGEMSCITCRCGA----------GVPHCERDD--
CHL2 vWC1 (33-75)      CLFGE-KIY-TPGQSWHPYL-EPQGTIYCVRCTCSEN--------GHVNCYRLR--
CHL2 vWC3 (248-289)    CTHNG-KTY-SHGEVWHPTV-LSFGPMPCILCTCID----------GYQDCHRVT--
```